

Efficient Maritime Healthcare Resource Allocation Using Reinforcement Learning

*Original*

Efficient Maritime Healthcare Resource Allocation Using Reinforcement Learning / Hasan, Tehreem; Batool, Farwa; Fiorino, Mario; Tretola, Giancarlo; Abbas, Musarat. - 39:(2024), pp. 615-620. ( 19th Conference on Computer Science and Intelligence Systems (FedCSIS) Belgrad (SRB) September 8–11, 2024) [10.15439/2024f8855].

*Availability:*

This version is available at: 11583/2994752 since: 2024-11-25T09:59:59Z

*Publisher:*

ACSIS

*Published*

DOI:10.15439/2024f8855

*Terms of use:*

This article is made available under terms and conditions as specified in the corresponding bibliographic description in the repository

*Publisher copyright*

(Article begins on next page)

# Damage detection in mooring systems of floating offshore wind turbines using semi-supervised GAN with image-transformed limited labelled data

Advances in Structural Engineering  
2025, Vol. 0(0) 1–19  
© The Author(s) 2025



Article reuse guidelines:  
[sagepub.com/journals-permissions](https://sagepub.com/journals-permissions)  
DOI: 10.1177/13694332251391469  
[journals.sagepub.com/home/ase](https://journals.sagepub.com/home/ase)



Pranjal Tamuly<sup>1,\*</sup> and Vincenzo Nava<sup>2</sup>

## Abstract

Detection of damage in the mooring systems of Floating Offshore Wind Turbines (FOWTs) is essential to guarantee operational reliability and reduce corrective maintenance costs. However, the complex nature of environmental conditions, the high costs of data collection, and the rarity of damage events make it challenging to obtain extensive labelled datasets. As a result, addressing damage detection from limited labelled data is necessary, yet it remains a relatively under-explored area in the literature. To tackle these challenges, this paper introduces an image-transformed semi-supervised generative adversarial network (ITSGAN) technique based on deep generative models. The method transforms time series data into multichannel image representations, enabling deep learning models to more effectively capture both spatial and temporal features. By combining adversarial training with supervised learning, ITSGAN leverages both labelled and unlabelled data to improve damage detection ability, particularly in scenarios where labelled data is scarce. A comparative analysis with established models such as traditional semi-supervised GAN, Deep Convolutional Neural Networks (DCNN), Support Vector Machines (SVM), and Extreme Gradient Boosting (XGB) shows that ITSGAN consistently outperforms these models in accuracy, precision, recall, and F1 score. It is also demonstrated that the proposed ITSGAN model preserves richer feature representations by transforming time series data into images, resulting in enhanced performance in damage detection tasks.

## Keywords

mooring system, generative adversarial network (GAN), floating wind turbine (FOWT), damage detection, semi-supervised learning

## Introduction

The transition to renewable energy sources is a critical component of global efforts to combat climate change and achieve sustainable energy goals, and wind energy is seen as one of the major players. In 2022, Europe witnessed a substantial surge in wind energy installations, boasting 19.1 GW of wind turbine infrastructure. In Europe and the UK, wind farms collectively generated 487 TWh of electricity, setting a record by meeting 17% of the total energy demand (WindEurope, 2023). In particular, offshore wind energy has experienced significant growth, with capacity increasing from 8503 MW in 2014 to 73,185 MW in 2023, highlighting the growing importance of the sector in meeting energy demands and reducing carbon emissions (International Renewable Energy Agency, 2024). Recent studies have shown that the amount of money spent on Operation and Maintenance (O&M) for offshore wind turbines is approximately 30% higher compared to onshore

wind turbines (Costa et al., 2021). This is because offshore wind turbines, especially floating ones, need to withstand severe environmental conditions, with their components subject to intense and fluctuating loads. Additionally, the accessibility of offshore wind farms for extended periods continues to pose a significant challenge for operation and maintenance activities.

A FOWT comprises various subsystems, including the tower, blades, gearbox, support structures, station-keeping,

<sup>1</sup>Basque Center for Applied Mathematics, Bilbao, Spain

<sup>2</sup>Department DIATI, Politecnico di Torino, Turin, Italy

\*Current affiliation: Department of Economics, Engineering, Society and Business Organisation, University of Tuscia, Viterbo, 01100, Italy.

## Corresponding author:

Pranjal Tamuly, Basque Center for Applied Mathematics, Alameda Mazarredo 14, Bilbao 48009, Spain.

Email: [ptamuly@bcmath.org](mailto:ptamuly@bcmath.org)

and electrical dispatch subsystems. In this study, our primary focus has been on mooring systems, which, despite being a critical component in terms of costs and reliability of floating offshore wind turbines, have received relatively less research attention. The study conducted by [Gordon et al. \(2014\)](#) showed that mooring system accidents related to mooring chain breakage exceeded 50% in the past two decades. Several incidents of mooring line failure have occurred in the last decade, with 4 of them having catastrophic outcomes ([Ma et al., 2013](#)). While these failures are associated with mooring systems in the oil and gas sector, it is important to acknowledge that the mooring systems of FOWTs experience similar damage conditions. However, the situation may be even more critical for FOWTs due to the lack of redundancy, which is typically much higher in the oil and gas industry. The potential for such failures to disrupt energy production, resulting in costly downtime, underscores the critical importance of proactive maintenance and early-stage damage detection.

Machine Learning (ML) and Artificial Intelligence (AI) have become leading methods for damage detection due to their capacity to analyze complex data and provide valuable insights. In this context, Deep Learning (DL) models are extensively employed for mooring line damage detection in the literature ([Yee et al., 2021](#)). For instance, multi-layer perceptrons (MLPs) are commonly used for damage assessment due to their implementation simplicity ([Sidarta et al., 2018](#)). Furthermore, [Gorostidi et al. \(2022\)](#) used synthetic data derived from various sea state simulations to train an MLP to identify mooring line damage in a semi-submersible platform. MLP was also used to predict wide-band fatigue damage in the mooring lines of a floating offshore wind turbine platform ([Li and Choung, 2017](#); [Li et al., 2018](#)). In the context of near real-time mooring line failure detection, Long Short-Term Memory (LSTM) was used alongside MLP ([Saad et al., 2021](#)). [Yao et al. \(2022\)](#) utilized a combined LSTM and PCA technique to detect anomalies in mooring lines, specifically when the anchor chain suffered damage at various positions. [Lee et al. \(2021\)](#) demonstrated the effectiveness of recurrent neural networks (RNNs) to detect damage in catenary mooring lines, achieving a high level of precision. [Janas et al. \(2021\)](#) introduced a convolutional neural network (CNN) based on images of the horizontal displacement history of the turret to detect the failure of the mooring line. They successfully differentiated between turret responses linked to intact and broken moorings using experimental simulations of operational scenarios. Also, [Sharma and Nava \(2024\)](#) developed a novel technique using a Convolutional Neural Network (CNN) combined with Auto-Regressive (AR) coefficients to monitor mooring systems. Recently, [Gorostidi et al. \(2023\)](#) proposed an autoencoder-based damage detection technique that takes inputs from time and frequency-domain statistics extracted from the platform's response under various metocean conditions.

Many of these existing deep learning applications in structural health monitoring primarily belong to the supervised learning category. These applications require a significant volume of labelled data to achieve the desired level of performance and accuracy. Acquiring extensive labelled datasets for supervised SHM techniques is a resource-intensive and labour-intensive process. In addition, finding well-annotated benchmark databases for damage detection and classification problems remains a challenge. This challenge arises primarily due to the rarity of recorded natural degradation and extreme events data. Hence, most of the data collected from the field belongs to the undamaged state of the structure, with very few representing the damaged state. The impact of limited labelled datasets on the performance of DL models in Structural Health Monitoring (SHM) has not been thoroughly studied.

Several common strategies are available in the literature to address the challenges of limited data. These strategies include Transfer Learning (TL), data augmentation, and oversampling ([Haixiang et al., 2017](#)). In transfer learning, a pre-trained model on similar data is fine-tuned for a new domain, reducing the need for a large amount of labelled data specific to the target domain ([Al-Stouhi and Reddy, 2016](#)). However, implementing Transfer Learning (TL) in SHM applications can be challenging because it requires access to a pre-trained and open-source model from a source dataset, which may not always be readily available. Data augmentation and oversampling involve increasing the data by artificial samples or applying specific transformations ([Gosain and Sardana, 2017](#)). However, this approach may generate highly correlated data, which sometimes leads to performance degradation ([Tarawneh et al., 2022](#)).

In addition to the conventional methods mentioned earlier, the use of Generative Adversarial Networks (GANs) is considered an alternative data augmentation approach. GANs generate entirely new synthetic data that the model has not encountered before, enhancing data diversity ([Engelmann and Lessmann, 2021](#)). [Gao et al. \(2019\)](#) introduced a data augmentation approach based on Deep Convolutional GANs (DCGANs) using a leaf-bootstrapping method for addressing a civil engineering problem. The application of progressive growth GAN was presented to create a diverse training database to improve road damage detection models ([Maeda et al., 2021](#)). However, applying GANs to augment the data in this way can be computationally expensive ([Gao et al., 2019](#)).

Another notable approach is GAN-based semi-supervised learning, which combines data generation and model training concurrently while harnessing the features of unlabelled data ([Odena, 2016](#)). [Gao et al. \(2021\)](#) employed a semi-supervised GAN for the classification of concrete cracking and spalling, demonstrating its remarkable effectiveness. Although a handful of applications of semi-supervised GANs exist in the field of damage

detection and classification; it is noteworthy that the majority of these applications are reliant on vision-based databases. The problem of detecting and classifying damage from limited time series data has not been thoroughly investigated. Specifically, there is a distinct lack of literature that addresses the specific challenge of detecting damage of mooring lines using limited labelled data. With this in mind, the objectives of this study are outlined below.

- To develop a deep learning-based approach that enhances damage detection accuracy in mooring systems for floating offshore wind turbines from limited timeseries labelled data.
- To propose and implement a semi-supervised learning model that leverages both labelled and unlabelled data effectively for identifying damage in offshore mooring systems.
- To assess the performance of semi-supervised generative adversarial networks in distinguishing various damage types (such as biofouling and anchor sliding) within FOWT mooring systems.
- To compare the effectiveness of the proposed semi-supervised approach with established machine learning models in detecting damage across multiple scenarios.

In this paper, an innovative image-transformed semi-supervised GAN (ITSGAN) is proposed to tackle the challenge of limited labelled data in mooring line damage detection and classification tasks. While semi-supervised GANs and time-series-to-image transformations have been explored individually, the core novelty of this work lies in their synergistic integration for the specific application of structural health monitoring in FOWT mooring systems. To the best of authors' knowledge, this is the first study to combine these techniques to address the critical issue of data scarcity in this domain. The proposed ITSGAN framework transforms one-dimensional time-history data into multi-channel image representations, enabling the deep learning model to capture complex spatial and temporal patterns that are often missed in the original time-series format. By coupling this transformation with a semi-supervised learning strategy, the model effectively leverages both the limited labelled data and the abundant unlabelled data. This integrated approach is shown to significantly improve damage detection accuracy, outperforming models that use either technique in isolation. This study demonstrates that the synergy between image transformation and semi-supervised learning offers a powerful solution for real-world SHM applications where obtaining labelled damage data is both costly and challenging.

This paper is organized as follows. First, the development of the floating wind turbine model is presented. Next, the proposed ITSGAN approach is introduced, followed by

a description of the dataset used to analyze various damage scenarios. The investigation strategy and the different machine learning models employed in the study are then discussed. Subsequently, the results and their implications are analyzed. Finally, the paper concludes with key findings and future research directions.

## Model development of FOWT

The deployment of floating wind turbines remains limited, and obtaining real data on wind turbine behaviour in operational conditions is challenging. In addition, the acquisition of operational data is further complicated by increased logistical costs, increased difficulties in data collection, and greater concerns about data privacy and security. Due to the scarcity of operational data, this study has incorporated the simulated response for damage classification purposes. Simulation of the response of wind turbines involves modelling the complex behaviour of turbines under diverse operating conditions by solving combinations of equations for fluid flow, aerodynamics, and structural dynamics. In this context, the National Renewable Energy Laboratory (NREL) has developed OpenFAST, which is an Open-source wind turbine simulation software framework for simulating the response of wind turbines under various operational scenarios. NREL and other researchers have conducted validation studies to ensure that the software accurately predicts the dynamic behaviour and response of wind turbines under various conditions (Coulling et al., 2013; Hsieh et al., 2021; Mendoza et al., 2022). Therefore, the adaptable and modular architecture of OpenFAST has been chosen to generate the response of the floating wind turbine platform. The modelling of NREL's 5 MW Baseline FOWT (Jonkman et al., 2009) mounted on the DeepCWind OC4 floater is explained in the following subsections.

### Floating platform model

The 5-MW DeepCwind semi-submersible foundation with a three-bladed rotor arrangement of a diameter of 126 m, as shown in Figure 1, has been extensively used for the design and analysis of floating wind turbines (Robertson et al., 2014) and it has been adopted as a numerical model in this work. Simulations of the numerical model of the FOWT system have been carried out in the time domain using the modular software OpenFAST.

### Wind turbine superstructure model

The DeepCWind design (Figure 1) consists of a central column and three peripheral offset columns. Additionally, an array of slender bracings is also introduced to enhance the structural rigidity of the floating structure. The

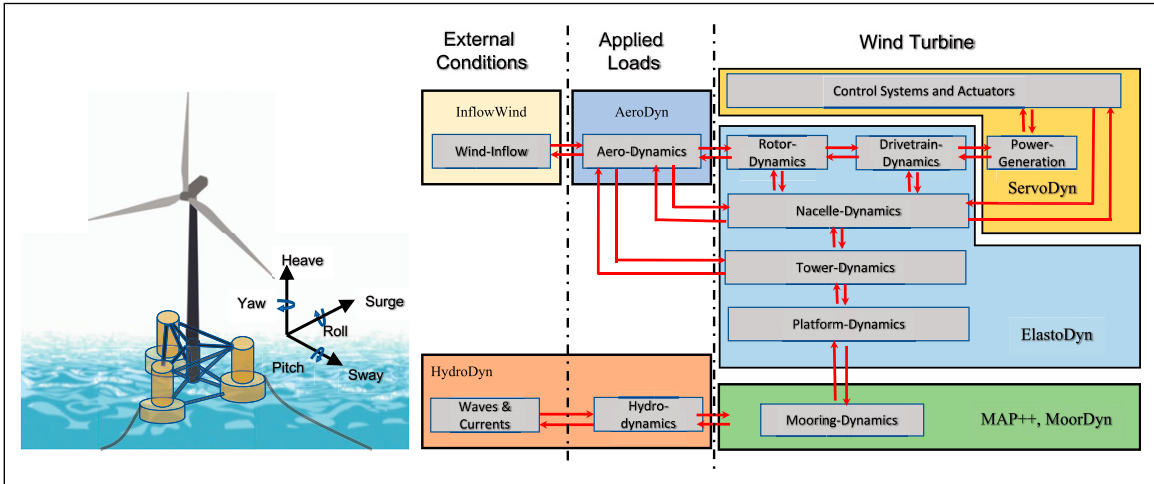


**Figure 1.** The DeepCwind semi-submersible platform features a three-bladed rotor configuration, accompanied by OpenFAST schematic illustrations.

HydroDyn module (Jonkman et al., 2014) of OpenFAST models the wave loading, current loading, and other hydrodynamic effects on the wind turbine structure and foundation.

The aerodynamics, consisting of rotor blade, nacelle and tower are modelled with the AeroDyn module of OpenFAST. This module calculates aerodynamic forces and loads along the length of each blade to maximize power output through blade pitch control. In addition, the ElastoDyn module focuses on modelling the structural dynamics of wind turbine components, including blades, towers, and the drivetrain. It encompasses a range of functions from calculating external loads imposed on the turbine due to wind conditions to modelling the behaviour of the control system. Additionally, the servo-hydraulic components of the control system are modelled using the

ServoDyn module to optimize power production and mitigate excessive loads.

*Mooring system model*

Mooring systems provide station-keeping to floating platforms and guarantee their range of functionality to safety limits. For this purpose, a set of three multi-point catenary chain mooring systems connected to the platform symmetrically 14.0 m below the mean sea level at fairleads, as shown in Figure 2. The mechanical characteristics of the mooring system in the DeepCWind concept are reported in Table 1. The global coordinates of the points where the anchor lines are attached to the floating platform and the seabed are given in Table 2. The MoorDyn module of the OpenFAST framework is

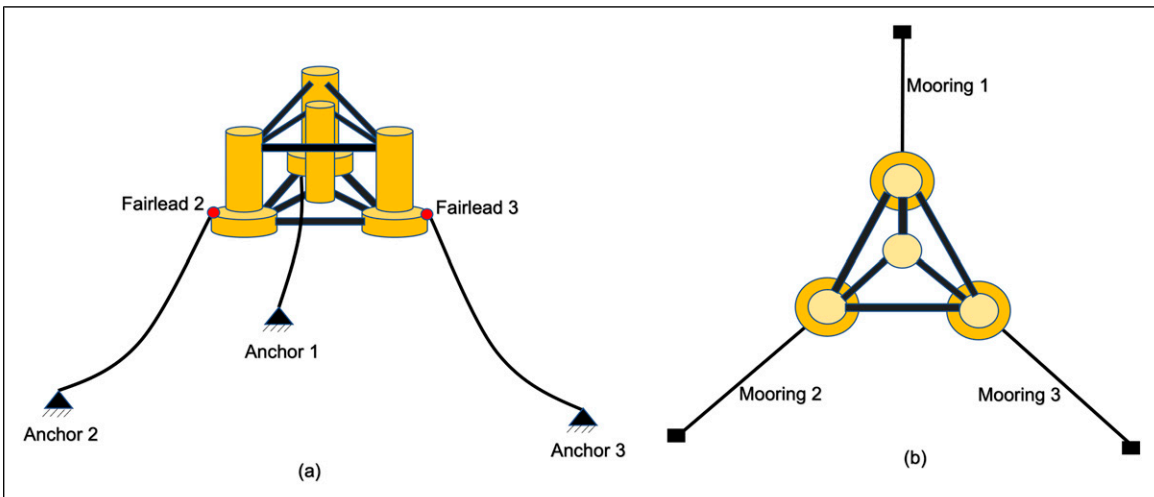


**Figure 2.** Multipoint mooring line configuration of floating platform (a) front view and (b) top view.

responsible for modelling the behaviour of the mooring system. It comprehensively accounts for mooring parameters such as stiffness, inertia, weight, buoyancy, damping, and seabed friction while representing the mooring dynamics. The interactions among different modules of OpenFAST, influenced by external conditions and applied loads, are illustrated in the schematic diagram in Figure 1.

## Dataset

The dataset for this investigation consists of both the undamaged and damaged states of the mooring system. There are two distinct damage scenarios considered in this study: biofouling and anchor sliding. A brief description of these different damage scenarios and their simulation framework is provided in the following subsection.

### Bio-fouling

Biofouling damage on mooring lines is a gradual process that can significantly impact the structural integrity and performance of FOWTs. As marine organisms colonize the surface of mooring lines, they create a biofilm that not only increases the overall weight of the lines but also introduces corrosive elements through the secretion of acids and enzymes. Over time, this biofilm can lead to accelerated structural degradation of the mooring lines. The attachment and growth of larger fouling organisms, such as barnacles and mussels, further exacerbate the problem by introducing

**Table 1.** Mooring line properties.

Line properties	Value
Mooring line diameter	0.0766 m
Mooring line length	835.5 m
Equivalent line Mass density in air	113.35 kg/m
Equivalent mooring line stiffness	$753.6 \times 10^6 \text{ Nm}^{-1}$
Seabed drag coefficient	1.0

**Table 2.** Global coordinates of the anchor (Fix) and the fairlead (Vessel) points.

Node		Node Co-ordinates		
Number	Node type	X	Y	Z
1	Fix	418.800	725.380	-200.000
2	Fix	-837.600	0.000	-200.000
3	Fix	418.800	-725.380	-200.000
4	Vessel	20.434	35.393	-14.000
5	Vessel	-40.868	0.000	-14.000
6	Vessel	20.434	-35.393	-14.000

Note. "Fix" represents the anchors, and "Vessel" represents the fairleads

additional weight, increasing hydrodynamic drag, and altering the surface roughness of the lines. These changes can compromise the load-bearing capacity of the lines, reduce their fatigue resistance, and increase the risk of failure, potentially threatening the offshore platform. The modular design of OpenFAST facilitates the integration of custom modifications within the MoorDyn module, enabling the simulation of damage scenarios in mooring systems. Specifically, to model biofouling damage, the mass per unit length of the mooring lines is increased while maintaining the original stiffness properties (Sharma and Nava, 2024; Tamuly et al., 2025). Biofouling in real-world scenarios can result in a significant range of mass increases, varying from minor (5%) to severe levels (over 50%) (Decurey et al., 2020). However, for this study, a minor damage range (5 – 10%) was selected to illustrate the efficiency of the proposed algorithm to detect subtle biofouling effects (Tamuly et al., 2025). Early detection of such damage is crucial for predictive maintenance, allowing timely interventions that prevent escalation. Additionally, the biofouling effect is applied uniformly to all mooring lines, as they are exposed to similar underwater conditions.

### Anchor sliding

In general, floating wind turbines are deployed in deep-sea conditions where conventional foundations cannot be constructed. Despite the challenges posed by deep waters, these wind turbines are anchored to the seabed to restrict their movements within a certain limit. The anchor mechanism ensures stability and prevents excessive drifting, enabling the effective operation of floating wind turbines. As the floating platform oscillates with wave and wind forces, the mooring lines experience dynamic tensions and movements. The anchor sliding problem occurs when anchors lose their holding capacity due to factors such as seabed conditions, extreme weather events, or inadequate embedment. The mooring dynamics (MoorDyn) module defines anchor positions by specifying the 3D coordinates of three anchor points on the seabed, particularly in the case of the DeepCwind platform (Table 2). These points are symmetrically placed on the vertices of an equilateral triangle on the seabed, contributing to overall stability. Like biofouling, a similar approach is adopted to generate the dataset for anchor failure. Specifically, the anchor point of a single mooring line along the wave direction is shifted within a range of (5 – 10) meter to mimic an anchor failure scenario (Tamuly et al., 2025).

Both undamaged and damaged simulated events generate six time-history responses corresponding to the platform's degrees of freedom (dofs): surge, sway, heave, roll, pitch, and yaw. A recent investigation by Sharma and Nava (2024) using a similar setup revealed that among these six dofs, the impact of mooring damage on the sway, roll, and yaw is minimal due to the structural symmetry and

**Table 3.** Training and testing datasets.

Dataset	State	Total samples	% Labelled data		
			5%	10%	20%
Training (12,000)	Biofouling	4000	200	400	800
	Anchor slippage	4000	200	400	800
	Undamaged	4000	200	400	800
Testing (300)	Biofouling	100	–	–	–
	Anchor slippage	100	–	–	–
	Undamaged	100	–	–	–

unidirectional application of external forces. Building on these findings, this study focuses on the three degrees of freedom most sensitive to mooring system damage—surge, heave, and pitch. For each metocean scenario, time-history responses for these three *dofs* are recorded over a duration of 820 seconds at a sampling frequency of 5 Hz. From these recordings, the last 320 seconds for each *dof* are retained to eliminate effects associated with the transient initial phase of 500 seconds.

The training dataset comprises 12,000 samples, capturing a range of system states under diverse environmental conditions, summarized in Table 4. Specifically, 4,000 unique combinations of environmental parameters are applied uniformly across all health states, including the undamaged (healthy) state, biofouling damage, and anchor slippage. This consistency in environmental conditions ensures that the analysis isolates the effects of damage on system responses, independent of external metocean variations. For testing, a separate dataset with 300 samples is prepared, consisting of 100 samples for each health state. Table 3 outlines the composition of the training and testing datasets, including subsets of labelled data corresponding to 5%, 10%, and 20% of the total samples.

### Transforming time-series data into grayscale images

The conversion of time series data into grayscale images presents several key advantages for the task of damage classification using CNN based models. By transforming time series data into grayscale images, temporal information within the time series is converted into a spatial format

**Table 4.** Simulation setup and environmental conditions.

Property	Value	Units
Simulation time	820	s
Sampling time step	0.20	s
Significant height, $H_S$	1–10	m
Peak period, $T_P$	7–15	s
Wind velocity, $V$	1–15	m/s
Current speed, $C$	0.5–1.5	m/s

to leverage CNN's ability to simultaneously detect both local and global patterns. This transformation facilitates faster and more efficient data processing, as CNNs are well-equipped to capture complex features across both spatial and temporal dimensions (Luczak, 2024).

Let  $x_i$  represent the time-series data for each sample, where  $i \in \{1, 2, 3\}$  denotes the three channels. To pre-process the image-transformed time-series data, each sample ( $x_i$ ) is centered by subtracting the mean ( $\mu$ ) of its corresponding channel, ensuring that the data is centered around zero, as follows:

$$\tilde{x}_i = x_i - \mu \quad (1)$$

Following centering, normalization is applied by scaling each channel's data based on the maximum absolute value within that channel, denoted as  $\max(|\tilde{x}_i|)$ , to constrain the values within a standard range of  $-1$  to  $1$ , as shown in the following equation:

$$\hat{x}_i = \frac{\tilde{x}_i}{\max(|\tilde{x}_i|)} \quad (2)$$

Next, each channel of the image-transformed time-series sample is reshaped into a  $40 \times 40$  matrix as follows:

$$M_i = \text{reshape}(\hat{x}_i, 40, 40) \quad (3)$$

Where  $x_i = \{x_{i1}, x_{i2}, \dots, x_{iT}\}$  is the original 1D time-series data, with  $T$  time steps. The reshaped matrix  $M_i$  is a  $40 \times 40$  matrix, where each element  $M_{ij}$  corresponds to an element from the original time series. Based on preliminary investigations, 1600 time steps are found to be optimal for reliable damage identification. Consequently, the choice of  $40 \times 40$  dimensions (since  $40 \times 40 = 1600$ ) ensures that all temporal information is preserved while enabling optimal compatibility with convolutional neural networks. Specifically, the matrix is populated as:

$$M_i = \begin{bmatrix} \hat{x}_{i1} & \hat{x}_{i2} & \cdots & \hat{x}_{i40} \\ \hat{x}_{i41} & \hat{x}_{i42} & \cdots & \hat{x}_{i80} \\ \vdots & \vdots & \ddots & \vdots \\ \hat{x}_{i1561} & \hat{x}_{i1562} & \cdots & \hat{x}_{i1600} \end{bmatrix} \quad (4)$$

Finally, the reshaped matrices  $M_1, M_2, M_3$  from each channel are combined to form a single three-channel grayscale image with dimensions  $40 \times 40 \times 3$ :

$$I = [M_1, M_2, M_3], \quad I \in \mathbb{R}^{40 \times 40 \times 3}. \quad (5)$$

This conversion of time series to images preserves temporal features by restructuring the sequential data into a spatial format while maintaining the temporal relationships. It preserves the sequential order of the data within each reshaped matrix capturing local temporal dependencies in its rows. This allows convolutional neural networks to learn temporal patterns by applying spatial filters to the transformed data. This method effectively maintains both local and global temporal dependencies, making it suitable for time-series analysis using image-driven models. Figure 3 illustrates both the

original and transformed form of a representative sample.

### Image-transformed semi-supervised GAN

Generative Adversarial Networks represent a groundbreaking paradigm in the realm of artificial intelligence and machine learning. It was first proposed by Ian Goodfellow (Goodfellow et al., 2020) and his collaborators. It has enabled the creation of remarkably realistic data that has found applications in art, design, image synthesis, and even scientific research. It consists of two neural networks, the generator and the discriminator, which compete against each other. Simultaneously training both networks enables them to navigate in a competitive environment, allowing them to optimize their weight parameters. The generator strives to

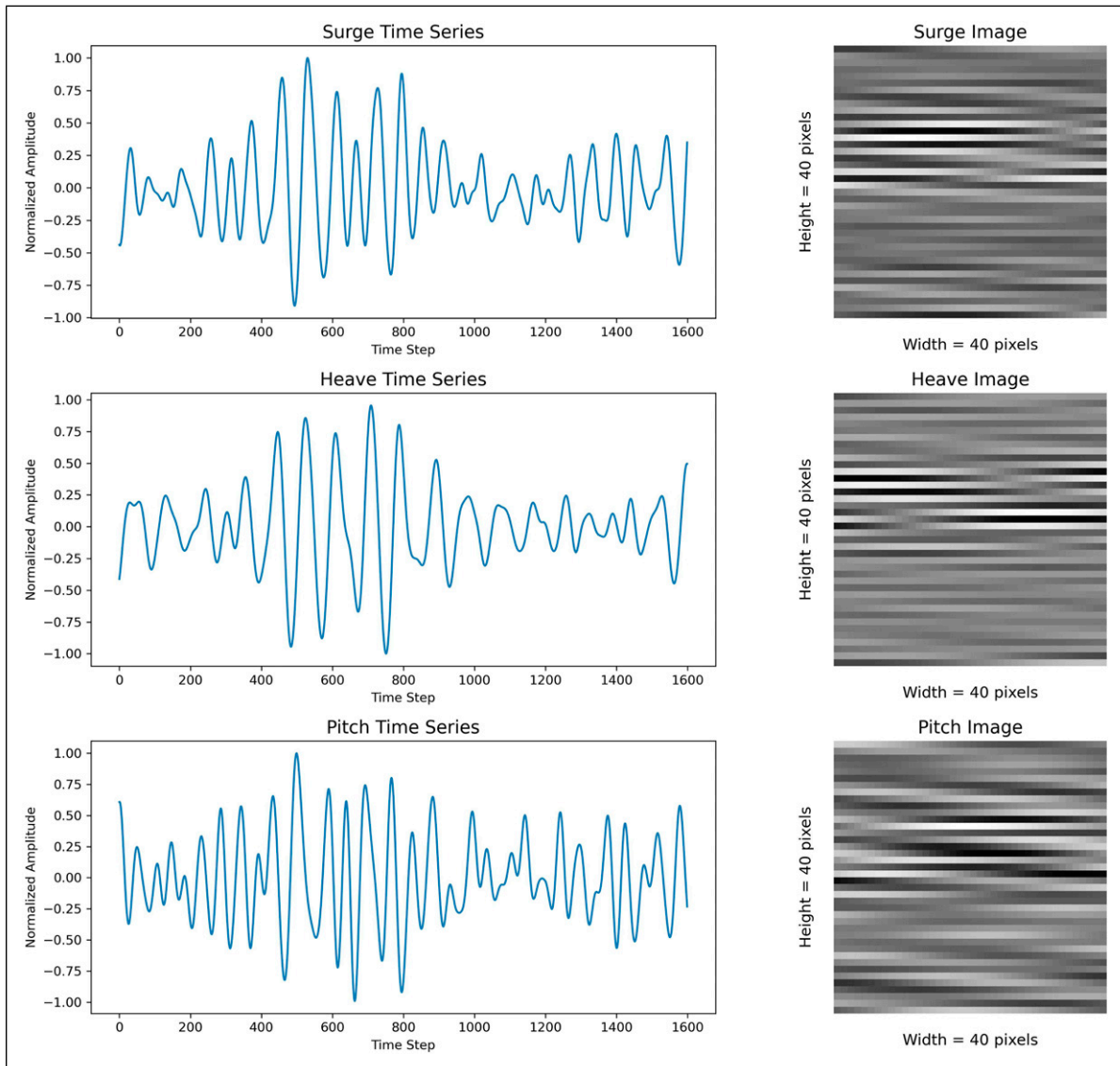


Figure 3. Conversion of normalized displacement timeseries to the corresponding image.

produce increasingly realistic data, while the discriminator aims to enhance its capacity to differentiate between real data and generated data.

Consider a  $d$ -dimensional space over real numbers, where  $x \in \mathbb{R}^d$  is a sample drawn from it. The GAN framework aims to approximate the real data distribution  $p_{data}$  by mapping a white noise vector  $\mathbf{z}$  of finite length sampled from the distribution  $p_z$ . The generator  $G$  with parameter  $\theta_G$  is trained to map the latent vector  $\mathbf{z}$  to synthesize a sample  $x_g = G(\mathbf{z}; \theta_G)$  to form the approximated distribution  $p_g$  of the real data. Conversely, the discriminator  $D$ , characterized by the parameters  $\theta_D$ , accepts an input image sample, either real or generated and its objective is to evaluate a probability score that distinguishes the origin of the sample, i.e., whether  $x$  comes from  $p_{data}$  or  $p_g$ . During the adversarial training process, both generator  $G$  and discriminator  $D$  aim to optimize the following Min-Max optimization problem.

$$\min_{\theta_G} \max_{\theta_D} \left\{ \mathbb{E}_{x \sim p_{data}} [\ln D(x)] + \mathbb{E}_{z \sim p_z} [\ln(1 - D(G(z)))] \right\} \quad (6)$$

where  $\mathbb{E}$  denotes the expectation operator. The first term,  $\mathbb{E}_{x \sim p_{data}} [\ln D(x)]$ , measures the average cross-entropy loss between the true labels (indicating real data) and the predicted probabilities from the discriminator when applied to real samples. Similarly, the term  $\mathbb{E}_{z \sim p_z} [\ln(1 - D(G(z)))]$  measures the cross-entropy loss between the true labels (indicating fake data) and the discriminator's predicted probabilities for the synthetic samples generated by the generator. In summary, the first term encourages the discriminator to recognize real data as real, while the second term drives the generator to produce samples that the

discriminator classifies as real. This adversarial training process continues until an optimum is reached or a predefined number of iterations is completed, resulting in the generator producing data that closely matches the real data distribution.

Although GANs are primarily known for their exceptional ability to generate realistic data [Li et al. \(2022\)](#), their application has been explored beyond data generation. One such application can be found for classification problems where labelled data is scarce or expensive to obtain, and traditional supervised learning approaches often produce unsatisfactory results. The Semi-supervised GANs (SGANs) emerge as an innovative solution for this problem by incorporating the learning from both labelled and unlabelled data to improve performance on classification tasks ([Odena, 2016](#)). Building upon these methodologies, we introduce the image-transformed Semi-Supervised GAN (ITSGAN), designed to improve damage detection tasks by harnessing the strengths of GANs trained on unlabelled data. This approach involves transforming multi-channel time series data into images, which are then analyzed using neural networks. The technique of converting time-series data into images for convolutional neural networks was first introduced by [Tang et al. \(2019\)](#) and has shown significant improvements. However, this approach has not been explored in the context of semi-supervised learning with Generative Adversarial Networks (GANs). In particular, the application of this method to damage detection in mooring lines has not yet been investigated.

The proposed framework involves two key objectives: a conventional adversarial goal and a supervised classification goal, as shown in [Figure 4](#). Initially, the

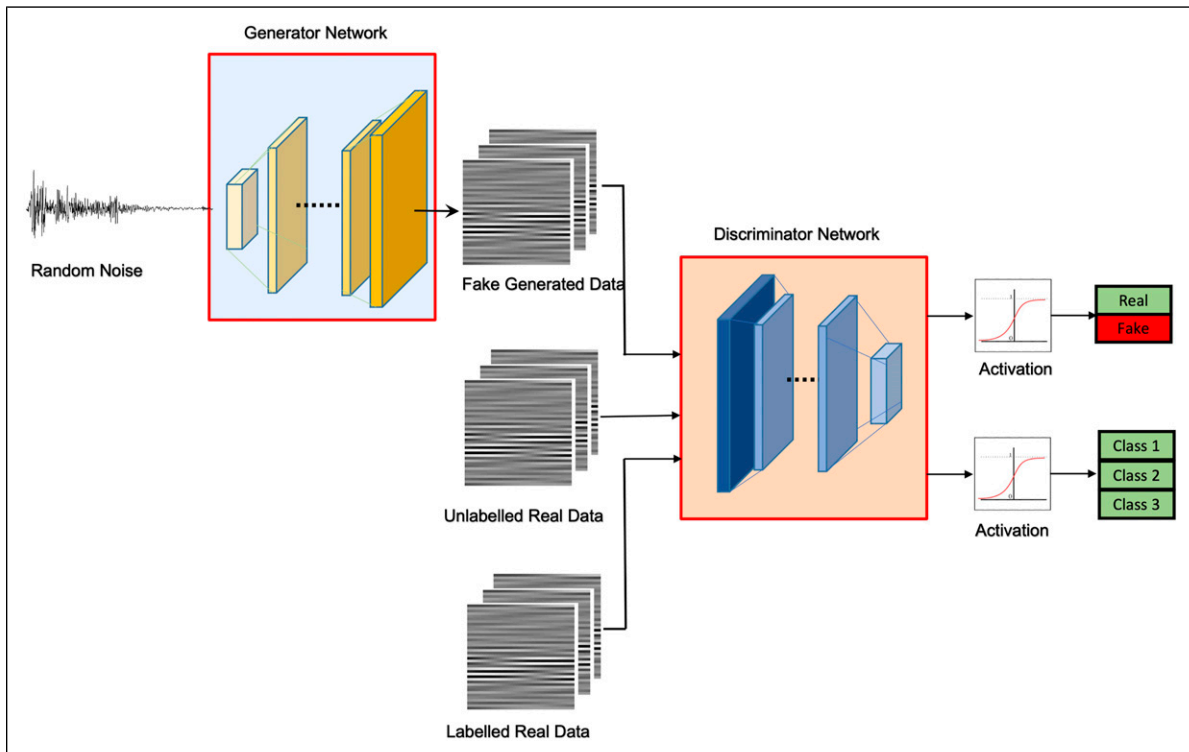


**Figure 4.** Framework of proposed ITSGAN.

generator is tasked with creating synthetic data that closely mimics real data, while the discriminator’s role is to differentiate between real and synthetic samples. Moreover, the discriminator is also trained on labelled data to identify and classify damage instances. This dual training approach enables the discriminator to learn a diverse set of features—one for distinguishing between real and synthetic data and another for performing classification tasks. The effectiveness of this method is further amplified by the shared feature learning between GAN training and the classification task. This synergy enhances the performance of the discriminator in damage detection, as it uses the rich and diverse features captured during adversarial training.

To achieve this, ITSGAN integrates the generated data into standard classifiers for  $K$  classes by assigning the generated samples to an additional class (i.e.,  $y = K + 1$ ), thus expanding the output dimension from  $K$  to  $K + 1$ . In this framework, the discriminator (or unsupervised classifier) produces a predictive probability vector  $p_{\text{model}}(y|x)$  of dimension  $K + 1$  for every input sample  $x$  drawn from either the real data distribution  $p_{\text{data}}$  or the generated data distribution  $p_g$ . Here,  $p_{\text{model}}(y = j|x)$  represents the estimated probability that the sample  $x$  belongs to the  $j$ -th class, where  $D(x)_1, \dots, D(x)_{K+1}$  are the logits associated with each class. In this context,  $p_{\text{model}}(y = K + 1|x)$  denotes the probability that the sample  $x$  is generated (i.e., fake). Therefore, we substitute  $D(x)$  in equation (6) with  $1 - p_{\text{model}}(y = K + 1|x)$  and  $1 - D(G(z))$  with  $p_{\text{model}}(y = K + 1|G(z))$ .

After substitution, the unsupervised loss  $L(D)_{\text{US}}$  is derived from equation (6) without relying on label information:

$$L(D)_{\text{US}} = -\mathbb{E}_{x \sim p_{\text{data}}} \ln(1 - p_{\text{model}}(y = K + 1 | x)) - \mathbb{E}_{x \sim p_g} \ln(p_{\text{model}}(y = K + 1 | x)) \quad (7)$$

The supervised discriminator incorporates label information and handles cases where the label  $y$  for real data is restricted to the  $K$  real classes (i.e.,  $y \in \{1, \dots, K\}$ ). Its supervised loss  $L(D)_S$  quantifies the cross-entropy between the actual distribution of labelled data  $p_{\text{data}}(x, y)$  and the predicted label distribution over the  $K$  classes:

$$L(D)_S = -\mathbb{E}_{x,y \sim p_{\text{data}}(x,y)} \ln(p_{\text{model}}(y | x, y < K + 1)) \quad (8)$$

Finally, the total discriminator loss is the summation of the supervised and unsupervised losses:

$$L(D) = L(D)_{\text{US}} + L(D)_S \quad (9)$$

Apart from the discriminator, the primary goal of the generator is to create synthetic data that is indistinguishable from real data. To accomplish this, the generator loss is formulated to measure the dissimilarity between the generated data and the real data distribution,

taking into account all  $K + 1$  classes. This loss can be expressed as:

$$L(G) = -\mathbb{E}_{z \sim p_z} \ln[1 - p_{\text{model}}(y = K + 1 | G(z))] \quad (10)$$

In this formulation, as summarized in Algorithm 1, the generator minimizes a binary cross-entropy loss to ensure that the generated samples are indistinguishable from real data. In contrast, the discriminator is trained using two types of loss. First, the supervised loss  $L(D)_S$  employs sparse categorical cross-entropy to accurately classify labelled real data, enabling effective damage classification. Second, the unsupervised loss  $L(D)_{\text{US}}$  is based on binary cross-entropy, where the discriminator learns to differentiate between real data and synthetic data generated by the generator.

Algorithm 1: ITSGAN

---

**Initialization:** Define Discriminator model  $D$  with weights  $\theta_D$   
 Define Generator model  $G$  with weights  $\theta_G$

**Training:**

```

for each epoch do for each batch do
    Sample a balanced batch of labelled real data:  $x_{\text{labelled}}$ 
    Sample a batch of real data (labelled + unlabelled):  $A^{\text{real}} = x_{\text{real}}$ 
    Sample noise vectors:  $\{z_1, z_2, \dots, z_n\} \sim p_z$ 
    Generate fake data:  $A^{\text{fake}} = \{G(z_1), G(z_2), \dots, G(z_n)\}$ 
    Compute unsupervised loss  $L(D)_{\text{US}}$  using  $A^{\text{real}}$  and  $A^{\text{fake}}$  (Eq. 7)
    Compute supervised loss  $L(D)_S$  using  $x_{\text{labelled}}$  (Eq. 8)
    Compute total discriminator loss:  $L(D) = L(D)_{\text{US}} + L(D)_S$ 
    Update  $\theta_D$ :  $\theta_D \leftarrow \theta_D - \eta_D \nabla_{\theta_D} L(D)$ 
    Compute generator loss  $L(G)$  using  $A^{\text{fake}}$  (Eq. 10)
    Update  $\theta_G$ :  $\theta_G \leftarrow \theta_G - \eta_G \nabla_{\theta_G} L(G)$ 
end
end
    
```

---

### Balanced batch sampling

Balanced Batch Sampling aims to improve performance during the supervised training phase by intelligently selecting data batches that maintain proportional representation across all classes. This approach addresses the common issue where machine learning models tend to be biased toward one class, resulting in poor performance on others and hindering the development of generalized models (Haixiang et al., 2017).

The process involves dynamically adjusting the composition of the mini-batch fed into the discriminator for classification (Gao et al., 2021). Suppose there are  $N$  samples drawn from  $K$  real classes in a mini-batch during supervised training. The balanced batch sampling ensures that each training batch contains an equal number of labelled samples from each class, i.e.,

$$n_1 = n_2 = \dots = n_K = \frac{N}{K}, \quad (11)$$

where  $n_1, n_2, \dots, n_K$  represent the number of samples per class. This technique helps the discriminator receive sufficient exposure to all classes, enhancing its ability to distinguish among them. It also indirectly benefits the generator by providing better feedback, thereby promoting

the synthesis of realistic and diverse data distributions across all classes.

### Network configurations

The input to the discriminator is a three-channel image representation of the image-transformed time series data, with dimensions of  $(N, 40, 40, 3)$ , where  $N$  represents the batch size and  $40 \times 40$  corresponds to the image dimensions. On the other hand, the input to the generator is a random noise vector sampled from a standard normal distribution, with dimensions of  $(N, 100)$ . The generator utilizes this noise to generate synthetic images that generate the time series data in image format, which are subsequently evaluated by the discriminator.

The architectural framework used in this study follows the principles established by Radford et al. (2015), which have been extensively used to develop deep convolutional GANs. In this framework, the discriminator is constructed using a sequence of strided convolutional layers that progressively reduce the spatial dimensions of the input while increasing its feature complexity. The discriminator accepts a three-channel image as input, followed by a succession of convolution operations. Specifically, the architecture consists of three distinct levels of feature extraction as shown in Table 5. Each level begins with a  $(3 \times 3)$  convolutional filters with a stride of  $(2,2)$  to downsample the data, followed by a  $(5 \times 5)$  convolutional filters with a stride of  $(1,1)$  for enhanced feature extraction. To combat overfitting, a dropout layer with a rate of 0.25 is applied after each feature extraction block. On the other hand, the generator starts with a Gaussian noise vector and slowly expands its dimension until it produces an output that matches the size of the discriminator input. The generator starts with a Gaussian noise vector and progressively performs upscaling operations. This process continues until the output dimensions align with the input

requirements specified for the discriminator, as detailed in Table 6. In its original implementation, transpose convolutional layers were utilized. However, this study employs the nearest-neighbour upsampling technique followed by convolutional layers which are found to be more effective approach (Florez et al., 2020). Each convolution operation is followed by ReLU activation except for the output layer of the generator, which uses the hyperbolic tangent activation function.

### Investigation framework

To comprehensively assess the ITSGAN algorithm, its performance is compared with several established machine learning models. This comparison aims to evaluate the strengths of ITSGAN in different scenarios and provide a thorough evaluation of its effectiveness. The benchmark models used for comparison include:

- **Deep Convolutional Neural Network (DCNN):** To rigorously assess the performance of the proposed ITSGAN algorithm, a Deep Convolutional Neural Network (DCNN) classifier is used as the primary benchmark due to its widespread use and demonstrated effectiveness in classification tasks. The DCNN classifier adopts the same architecture as the discriminator model in the ITSGAN framework, as outlined in Table 5. The model replaces 2D convolution with 1D convolution layers without any transformation of the timeseries data. This alignment ensures a fair and consistent basis for evaluating the ITSGAN performance.
- **Semi-Supervised Generative Adversarial Network (SGAN):** To evaluate the effectiveness of the proposed transformation over the ITSGAN framework, a traditional Semi-Supervised Generative Adversarial Network (SGAN) is employed for

**Table 5.** Architecture details of the discriminator.

Layer	Name	Kernel (Filter)	Activation	Shape	Remarks
Input	–	–	–	$(N, 40, 40, 3)$	Input time-series transformed to image
Conv2D	Conv1	$3 \times 3$ (128)	Leaky ReLU ( $\alpha = 0.2$ )	$(N, 20, 20, 128)$	Stride = (2, 2)
Conv2D	Conv2	$5 \times 5$ (256)	Leaky ReLU ( $\alpha = 0.2$ )	$(N, 20, 20, 256)$	Stride = (1, 1)
Dropout	Drop1	–	–	$(N, 20, 20, 256)$	Dropout rate = 0.25
Conv2D	Conv3	$3 \times 3$ (256)	Leaky ReLU ( $\alpha = 0.2$ )	$(N, 10, 10, 256)$	Stride = (2, 2)
Conv2D	Conv4	$5 \times 5$ (256)	Leaky ReLU ( $\alpha = 0.2$ )	$(N, 10, 10, 256)$	Stride = (1, 1)
Dropout	Drop2	–	–	$(N, 10, 10, 256)$	Dropout rate = 0.25
Conv2D	Conv4	$3 \times 3$ (256)	Leaky ReLU ( $\alpha = 0.2$ )	$(N, 5, 5, 256)$	Stride = (2, 2)
Conv2D	Conv5	$5 \times 5$ (256)	Leaky ReLU ( $\alpha = 0.2$ )	$(N, 5, 5, 256)$	Stride = (1, 1)
Dropout	Drop3	–	–	$(N, 5, 5, 256)$	Dropout rate = 0.25
Conv2D	Conv6	$3 \times 3$ (128)	Leaky ReLU ( $\alpha = 0.2$ )	$(N, 5, 5, 128)$	Stride = (1, 1)
Flatten	Flatten_1	–	–	$(N, 3200)$	$5 \times 5 \times 128 = 3200$
Fc-layer	FC1	–	Softmax	$(N, C)$	SGAN: $C = K + 1$ ; DCNN: $C = K$

**Table 6.** Configuration of the generator.

Layer	Kernel (Filter)	Activation	Shape	Remarks
Input	–	–	(N, 100)	Noise from standard normal distribution
Fc-layer	–	ReLU	(N, 500)	–
Reshape	–	–	(N, 10, 10, 5)	–
Up-sampling	–	–	(N, 20, 20, 5)	Stride=(2,2), interpolation = nearest-neighbour
Conv2D	3 × 3 (32)	ReLU	(N, 20, 20, 32)	Stride=(1,1)
BatchNorm	–	–	(N, 20, 20, 32)	Momentum = 0.8
Conv2D	5 × 5 (32)	ReLU	(N, 20, 20, 32)	Stride=(1,1)
BatchNorm	–	–	(N, 20, 20, 32)	Momentum = 0.8
Up-sampling	–	–	(N, 40, 40, 32)	Stride=(2,2), interpolation = nearest-neighbour
Conv2D	3 × 3 (32)	ReLU	(N, 40, 40, 32)	Stride=(1,1)
BatchNorm	–	–	(N, 40, 40, 32)	Momentum = 0.8
Conv2D	5 × 5 (32)	ReLU	(N, 40, 40, 32)	Stride=(1,1)
BatchNorm	–	–	(N, 40, 40, 32)	Momentum = 0.8
Conv2D	3 × 3 (3)	Tanh	(N, 40, 40, 3)	Stride=(1,1)

comparative analysis. The SGAN framework utilizes an architecture for its discriminator and generator models that is identical to that of the ITSGAN, with the key distinction being the use of 1D convolution operations instead of 2D convolutions. It directly processes multivariate time-series data without any transformations, except for the normalization step used in ITSGAN, ensuring a more relevant comparison. By employing this approach, we aim to demonstrate the advantages of the proposed transformation over the ITSGAN, specifically in the context of damage detection of the mooring system.

- **Support Vector Machine Classifier (SVM):** The Support Vector Machine (SVM) is a robust and widely used traditional classification model. Comparing ITSGAN with SVM allows us to assess whether the generative capabilities and transformations introduced by ITSGAN provide significant advantages over this conventional approach. Since SVM is effective in finding optimal class boundaries, it serves as a strong baseline to evaluate the performance improvements ITSGAN offers.
- **Extreme Gradient Boosting Classifier (XGB):** XGBoost is a cutting-edge tree-based algorithm recognized for its exceptional performance and flexibility in handling various types of data. It is particularly effective at capturing intricate patterns through gradient-boosted decision trees, making it one of the most advanced models in its category. By comparing ITSGAN to XGBoost, it is aimed to determine the effectiveness of ITSGAN over this powerful traditional classifier. The XGBoost classifier is set with 100 estimators and a maximum depth of 10.

It is important to clarify the training data usage for fair comparison between supervised and semi-

supervised approaches. The supervised models (DCNN, SVM, and XGB) are trained exclusively using only the labelled data subsets (5%, 10%, or 20% of total samples) as specified in Table 3. In contrast, the semi-supervised models (ITSGAN and SGAN) utilize both labelled and unlabelled data during training, where the discriminators are trained with dual objectives: supervised classification using the labelled subset and adversarial learning using both labelled and unlabelled to distinguish real from generated samples. This training strategy ensures a methodologically sound comparison that demonstrates the advantage of semi-supervised learning in effectively leveraging additional unlabelled data that supervised models cannot utilize. For each scenario, the training duration for all models is extended to 250 epochs with batch size of 512. The Adam optimizer is utilized with an initial learning rate of  $2 \times 10^{-4}$ . All experiments are executed on the TensorFlow platform, utilizing the Donostia International Physics Center supercomputing facility, which is equipped with an NVIDIA Tesla P40 GPU. This computational setup ensures efficient handling of the extensive training requirements.

### Performance evaluation metrics

The performance of the proposed ITSGAN algorithm is assessed using standard classification metrics. These metrics are derived from the elements of the confusion matrix: True Positives (TP), True Negatives (TN), False Positives (FP), and False Negatives (FN). In this context, TP denotes correctly identified positive instances, TN denotes correctly identified negative instances, FP refers to negative instances incorrectly classified as positive, and FN refers to positive instances incorrectly classified as negative. **Accuracy** is used to evaluate the overall correctness of the model across all classes and is defined as:

$$\text{Accuracy} = \frac{\sum_{i=1}^k TP_i}{N} \quad (12)$$

Here,  $n_i$  is the number of samples in class  $i$ ,  $k$  is the total number of classes, and  $N = \sum_{i=1}^k n_i$  is the total number of samples in the test set. **Precision** quantifies the proportion of correctly identified positive predictions among all positive predictions. For multi-class classification, weighted averaging is employed, which computes the metric for each class and averages them weighted by the number of samples in each class:

$$\text{Precision} = \sum_{i=1}^k \frac{n_i}{N} \cdot \frac{TP_i}{TP_i + FP_i} \quad (13)$$

Weighted averaging is chosen as it provides a more representative performance measure by accounting for class distribution, ensuring that classes with more samples have proportional influence on the final metric. This approach is particularly robust and provides meaningful results regardless of whether the dataset is perfectly balanced or has class imbalances. **Recall** indicates the proportion of correctly identified positive instances among all actual positives. Using weighted averaging, recall is computed as:

$$\text{Recall} = \sum_{i=1}^k \frac{n_i}{N} \cdot \frac{TP_i}{TP_i + FN_i} \quad (14)$$

**F1 Score** is employed as the harmonic mean of precision and recall, providing a balanced evaluation of the model's predictive capability. The weighted F1 score is calculated as:

$$F_1 = \sum_{i=1}^k \frac{n_i}{N} \cdot \frac{2 \times \text{Precision}_i \times \text{Recall}_i}{\text{Precision}_i + \text{Recall}_i} \quad (15)$$

## Results and discussions

A systematic comparative analysis is conducted to evaluate the performance of the proposed ITSGAN algorithm in relation to models described in the preceding section. The evaluation employs various performance metrics, including accuracy, precision, recall, and F1 score, to measure their effectiveness in detecting and classifying damage across multiple classes in the test dataset.

The performance trends in Table 7 reveal critical insights into the limitations of different models, particularly in low-data scenarios. A clear pattern emerges where models relying purely on supervised learning, such as SVM, XGBoost, and DCNN, struggle significantly with only 5% labelled data. The extremely low accuracy of SVM and XGBoost highlights their dependency on sufficient labelled samples for effective feature learning. Even DCNN, despite its deep learning architecture, achieves only 58.7%, indicating the challenges of training

**Table 7.** Performance metrics for various models with different percentages of labelled data.

% Labelled data	Model	Accuracy	Precision	Recall	F <sub>1</sub>
5%	ITSGAN	68.3	68.4	68.3	68.4
	SGAN	45.3	45.3	45.3	44.9
	DCNN	58.7	58.2	58.7	58.2
	SVM	31.3	29.8	31.3	29.5
	XGB	43.7	43.4	43.7	43.4
10%	ITSGAN	83.7	84.0	83.7	83.8
	SGAN	67.7	68.5	67.7	68.0
	DCNN	71.3	70.8	71.3	70.2
	SVM	35.3	34.8	35.3	34.6
	XGB	56.0	56.5	56.0	56.1
20%	ITSGAN	92.0	91.9	92.0	91.9
	SGAN	84.0	84.0	84.0	84.0
	DCNN	86.0	86.0	86.0	85.7
	SVM	39.0	39.2	39.0	39.0
	XGB	67.3	67.4	67.3	67.3

deep networks with minimal supervised samples. On the other hand, ITSGAN outperforms all models achieving 68.3% accuracy, effectively leverages both labelled and unlabelled data through adversarial and supervised learning objectives. While SGAN employs a similar semi-supervised approach without any transformation, it fails to achieve comparable performance to ITSGAN, indicating limited ability to leverage unlabelled data as effectively as ITSGAN.

As labelled data increases to 10% and 20%, all models improve, but the performance gaps between them remain notable. While ITSGAN benefits significantly from additional labelled data (rising to 83.7% and then 92.0%), traditional models like SVM and XGBoost continue to struggle. The trend also highlights a limitation of SGAN, as its performance did not surpass that of DCNN. This suggests that semi-supervised learning alone is insufficient unless combined with an effective strategy, such as image transformation to enhance feature extraction for the classification task. The trends in precision, recall, and F1-score closely follow the accuracy patterns across different models and labelled data percentages. ITSGAN consistently achieves a better balance between precision and recall, resulting in superior F1-scores across all data settings. This highlights the crucial role of the proposed transformation in semi-supervised learning in enhancing classification performance, particularly in low-data scenarios.

The confusion matrices presented in Figures 5–7 provide a detailed comparison of model performance for the 5%, 10%, and 20% labelled data scenarios, respectively. These matrices visualize the classification accuracy for the Undamaged (UD), Anchor Slippage (AN), and Biofouling (BF) damage states, offering insights into how well each model distinguishes between different health conditions as data availability increases.

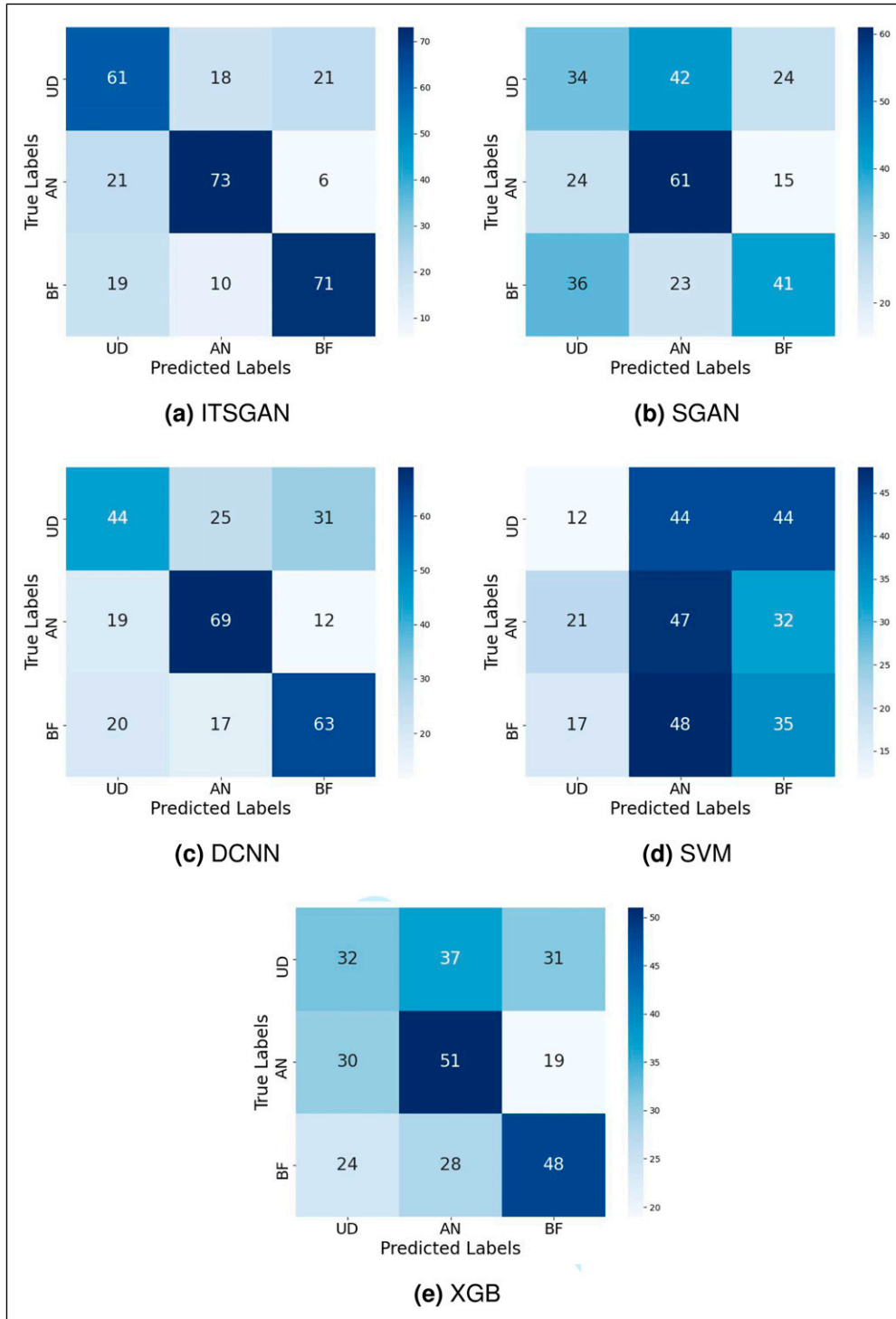


**Figure 5.** Confusion matrices for different models trained on 5% labelled input data.

In the highly constrained 5% labelled data scenario (Figure 5), most models exhibit significant confusion between the classes. The proposed ITSGAN, however, demonstrates the most robust performance by achieving the best class separation among the models. In contrast, traditional supervised models like SVM and XGBoost show

widespread misclassification, often failing to distinguish effectively between damaged and undamaged states. The DCNN and SGAN models perform moderately but still show considerable overlap between the damage classes.

As the proportion of labelled data increases to 10% (Figure 6), a clear improvement in classification accuracy is

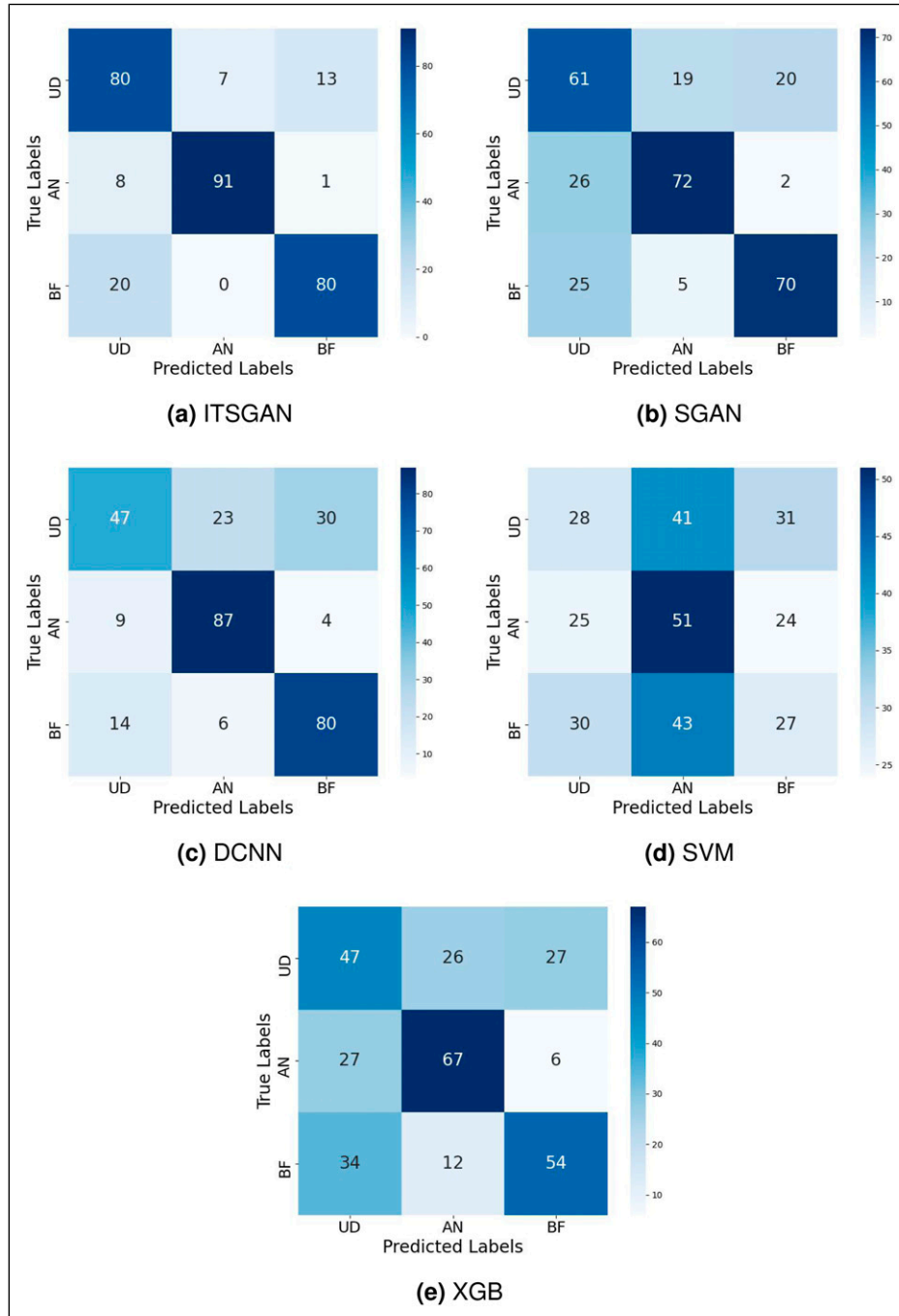


**Figure 6.** Confusion matrices for different models trained on 10% labelled input data.

observed across all deep learning models. ITSGAN, in particular, shows a substantial reduction in inter-class confusion. The DCNN also shows marked improvement, though it still exhibits more misclassifications than ITSGAN. The performance of SVM and XGBoost remains limited, highlighting the challenge for traditional models in learning from sparse datasets.

At the 20% labelled data level (Figure 7), ITSGAN achieves a high degree of classification accuracy, with

minimal confusion between the damage states. While the DCNN model's performance becomes more competitive, ITSGAN's ability to distinguish all classes remains superior, particularly in correctly identifying the subtle biofouling damage. The other models, SGAN, SVM, and XGB, continue to exhibit higher misclassification rates, underscoring the combined advantage of ITSGAN's image-transformation and semi-supervised learning framework.

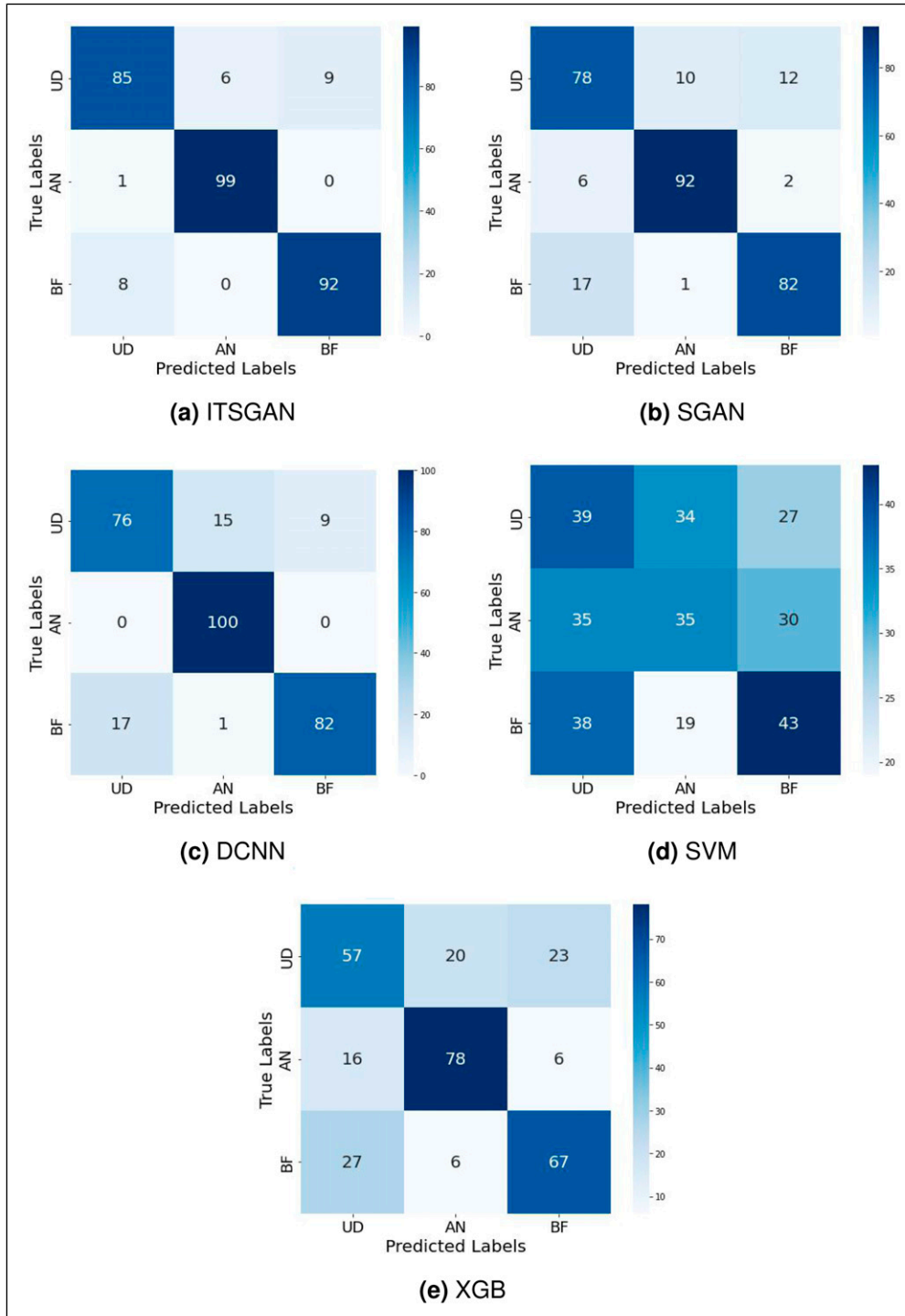


**Figure 7.** Confusion matrices for different model figures trained on 20% labelled input data.

A consistent trend observed across all scenarios is that AN damage is more distinctly classified than BF damage, suggesting that anchor slippage produces a more recognizable signature in the platform’s dynamic response. The progressive analysis from 5% to 20% highlights the key strength of the proposed ITSGAN framework. The semi-

supervised approach using image-transformed data allows it to effectively leverage unlabelled data, ensuring stable and superior performance in low-data regimes where traditional supervised methods falter. Overall, these results confirm the effectiveness of ITSGAN in capturing complex damage patterns and reveal the limitations of

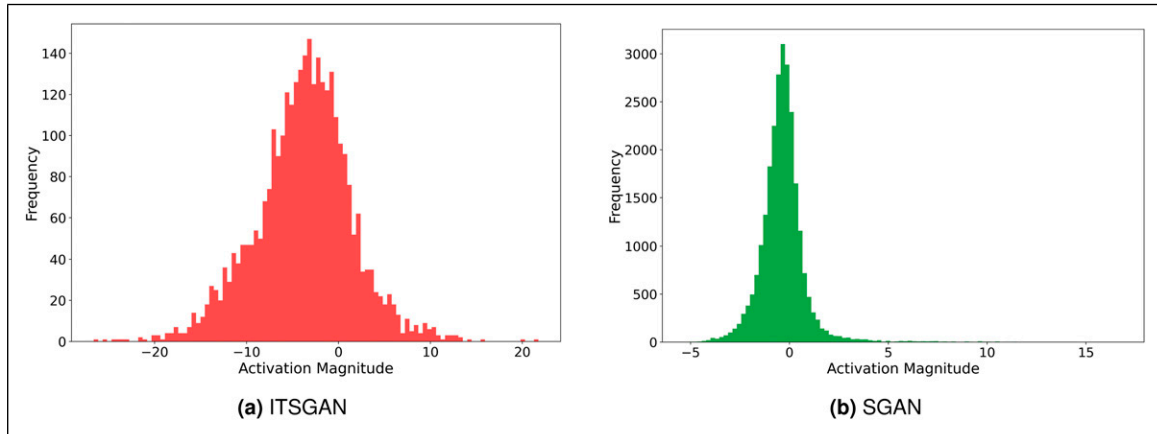


**Figure 8.** Comparison of activation histograms for Conv6 layer.

conventional machine learning approaches for this SHM task.

To explore the performance of the proposed ITSGAN with the traditional SGAN model more closely, activation histograms of feature spaces are generated using a randomly selected test sample for both the ITSGAN and SGAN models. Figure 8 shows activation histograms for the Conv6 layer, as detailed in Table 5. In our network architecture, Conv6 represents the final convolutional layer before the output is flattened and passed to the fully connected classification layer. The activations at this stage capture the most abstract and high-level features extracted from the input data, as they result from successive transformations and nonlinearities applied by the preceding convolutional layers. Analyzing the activation distribution at this depth provides valuable insight into the richness and diversity of the learned feature representations, which are directly responsible for the model's classification performance. Further, the Conv6 layer is the last point in the network where spatial information is preserved before the transition to the dense output layer.

This makes it an ideal candidate for comparing how different models (such as ITSGAN and SGAN) encode and utilize spatial and temporal patterns in the data. The  $x$ -axis of Figure 8 denotes the magnitude of activations and the  $y$ -axis denotes the frequency of activations. The activation distributions for ITSGAN and SGAN reveal critical insights into their feature representations. ITSGAN exhibits a wider and more symmetric activation distribution, with magnitudes spanning a broader range. This suggests that ITSGAN is capable of learning more diverse and discriminative features, which contributes to its superior performance. In contrast, activation distribution of SGAN is more concentrated around zero with a sharp peak, indicating limited feature diversity and weaker activation responses. This indicates that SGAN struggles to extract diverse meaningful representations, leading to its relatively lower classification performance. The broader range of activations in ITSGAN highlights the effectiveness of the proposed transformation strategy, which allows ITSGAN to extract richer and more discriminative features. Despite sharing the same number of

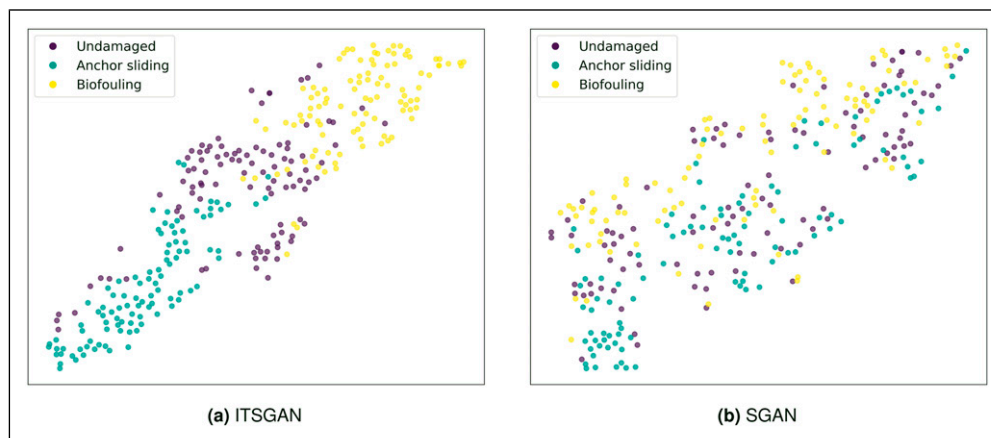


**Figure 9.** t-SNE plot for the testing data using the models trained on 20% labelled data.

convolutional layers and adversarial training strategy as SGAN, ITSGAN captures a wider activation range, suggesting that the proposed image transformation enhances feature learning.

To further investigate their performance, t-SNE (t-Distributed Stochastic Neighbour Embedding) (Van der Maaten and Hinton, 2008) technique is applied to reduce dimensionality and visualize high-dimensional data in a lower-dimensional space. The resulting t-SNE plot for the testing data using the trained ITSGAN model is illustrated in Figure 9. The t-SNE plot visualizes the feature space of the dataset after applying dimensionality reduction. The SGAN models exhibit significant class overlap and poor separation, resulting in weak performance in distinguishing damage types. ITSGAN improves separation but still shows some mixing between the anchor and biofouling states. However, ITSGAN effectively forms distinct and well-separated clusters for each class with minimal overlap, improving latent feature extraction and enhancing damage detection accuracy.

## Conclusions

This paper introduces a semi-supervised GAN-based approach for detecting damage in floating offshore wind turbine mooring systems, addressing the challenge of limited labelled data. The proposed ITSGAN framework enhances the traditional machine learning based approach by adapting it specifically for time-series data driven damage detection of mooring systems. The proposed transformation of time-series data into images captures complex patterns and spatial relationships, while utilizing GANs in a semi-supervised setting to address the challenge of limited labelled data. These advancements make the method particularly effective in overcoming the limitations of traditional techniques in damage detection using limited labelled data. The key conclusions drawn from this study are outlined below:

- ITSGAN algorithm consistently outperforms the established models, demonstrating superior accuracy and robustness across different data availability scenarios. Its ability to maintain high performance underscores the effectiveness of proposed ITSGAN to leverage both labelled and unlabelled data effectively for damage detection task.
- The results underscore the crucial role of the proposed data transformation in enhancing feature extraction and classification performance. These findings demonstrate that a well-designed semi-supervised approach can significantly improve damage detection in floating offshore wind turbine mooring systems. Furthermore, the study suggests that while semi-supervised learning is beneficial, it is insufficient on its own; an effective data

transformation strategy is essential for optimal feature extraction. Notably, despite employing the same number of convolutional layers, ITSGAN outperforms SGAN, highlighting the significant impact of the transformation process on model performance.

- The analysis of activation histograms for the same convolution layers for both ITSGAN and SGAN models reveals significant differences. The ITSGAN model displays a broader range of activations, with values spanning a wider spectrum compared to the SGAN model. This wider spread suggests that ITSGAN is more effective in utilizing the full dynamic range of its activation functions, capturing more diverse and complex feature representations.
- The t-SNE analysis shows that ITSGAN creates clearer class separation compared to SGAN, which struggles with significant overlap. While some mixing remains between the anchor and biofouling states, ITSGAN still improves feature extraction and classification accuracy.

This study is based on numerical experiments conducted on the DeepCWind 5 MW FOWT with aligned wave, wind, and current directions. Further research is needed to assess how misalignment affects the behaviour of the platform across different degrees of freedom. Additionally, the biofouling damage modelling assumes uniform mass distribution along the mooring lines, whereas real-world biofouling typically exhibits spatial variability and may affect both mass and stiffness properties. Since the analysis relies only on simulated data, real-world validation is crucial to confirm the method's effectiveness and practical applicability.

The practical deployment of ITSGAN may involve integration with existing structural health monitoring systems, where continuous sensor data streams can be transformed into image representations for real-time damage detection. However, challenges such as sensor noise, data heterogeneity, and the need for robust pre-processing pipelines must be addressed. Future work should also explore the performance of ITSGAN on naturally imbalanced real-world datasets to further assess its robustness and generalization capabilities. Overall, the proposed ITSGAN shows promising results for damage detection using time-series data, where labelled data is limited.

## ORCID iDs

Pranjal Tamuly  <https://orcid.org/0000-0001-6511-5974>

Vincenzo Nava  <https://orcid.org/0000-0002-3207-3517>

## Funding

The authors disclosed receipt of the following financial support for the research, authorship, and/or publication of this article: The

authors also would like to acknowledge the ELKARTEK project RUL-ET funded by the Basque Government (KK-2024/00086); the “BCAM Severo Ochoa” accreditation of excellence CEX2021-001142-S/MICIN/AEI/10.13039/501100011033; and the Basque Government through the BERC 2022-2025 program. The authors also express their gratitude to the Donostia International Physics Center (DIPC) team for their collaboration and assistance in providing high-performance computing (HPC) resources.

### Declaration of conflicting interests

The authors declared no potential conflicts of interest with respect to the research, authorship, and/or publication of this article.

### References

- Al-Stouhi S and Reddy CK (2016) Transfer learning for class imbalance problems with inadequate data. *Knowledge and Information Systems* 48: 201–228.
- Costa ÁM, Orosa JA, Vergara D, et al. (2021) New tendencies in wind energy operation and maintenance. *Applied Sciences* 11(4): 1386.
- Coulling AJ, Goupee AJ, Robertson AN, et al. (2013) Validation of a fast semi-submersible floating wind turbine numerical model with deepwind test data. *Journal of Renewable and Sustainable Energy* 5(2): 023116.
- Decurey B, Schoefs F, Barillé AL, et al. (2020) Model of bio-colonisation on mooring lines: updating strategy based on a static qualifying sea state for floating wind turbines. *Journal of Marine Science and Engineering* 8(2): 108.
- Engelmann J and Lessmann S (2021) Conditional WassersteinGAN-based oversampling of tabular data for imbalanced learning. *Expert Systems with Applications* 174: 114582.
- Florez MA, Caporale M, Buabthong P, et al. (2020) Data-driven accelerometer synthesis using deep generative models. *arXiv preprint arXiv:2011.09038*.
- Gao Y, Kong B and Mosalam KM (2019) Deep leaf-bootstrapping generative adversarial network for structural image data augmentation. *Computer-Aided Civil and Infrastructure Engineering* 34(9): 755–773.
- Gao Y, Zhai P and Mosalam KM (2021) Balanced semi-supervised generative adversarial network for damage assessment from low-data imbalanced-class regime. *Computer-Aided Civil and Infrastructure Engineering* 36(9): 1094–1113.
- Goodfellow I, Pouget-Abadie J, Mirza M, et al. (2020) Generative adversarial networks. *Communications of the ACM* 63(11): 139–144.
- Gordon RB, Brown MG and Allen EM (2014) Mooring integrity management: a state-of-the-art review. In: *Offshore Technology Conference*. OTC, D041S047R006.
- Gorostidi N, Nava V, Aristondo A, et al. (2022) Predictive maintenance of floating offshore wind turbine mooring lines using deep neural networks. *Journal of Physics: Conference Series* 2257: 012008.
- Gorostidi N, Pardo D and Nava V (2023) Diagnosis of the health status of mooring systems for floating offshore wind turbines using autoencoders. *Ocean Engineering* 287: 115862.
- Gosain A and Sardana S (2017) Handling class imbalance problem using oversampling techniques: a review. In: *2017 International Conference on Advances in Computing, Communications and Informatics (ICACCI)*. IEEE, 79–85.
- Haixiang G, Yijing L, Shang J, et al. (2017) Learning from class-imbalanced data: review of methods and applications. *Expert Systems with Applications* 73: 220–239.
- Hsieh AS, Brown KA, DeVelder NB, et al. (2021) High-fidelity wind farm simulation methodology with experimental validation. *Journal of Wind Engineering and Industrial Aerodynamics* 218: 104754.
- International Renewable Energy Agency (IRENA) (2024) *Renewable Energy Statistics 2024*. International Renewable Energy Agency.
- Janas K, Milne I and Whelan J (2021) Application of a convolutional neural network for mooring failure identification. *Ocean Engineering* 232: 109119.
- Jonkman J, Butterfield S, Musial W, et al. (2009) *Definition of a 5-mw Reference Wind Turbine for Offshore System Development*. Technical report, National Renewable Energy Laboratory. <https://www.osti.gov/biblio/947422>
- Jonkman JM, Robertson A and Hayman GJ (2014) *Hydrodynamics User's Guide and Theory Manual*. National Renewable Energy Laboratory.
- Lee K, Chung M, Kim S, et al. (2021) Damage detection of catenary mooring line based on recurrent neural networks. *Ocean Engineering* 227: 108898.
- Li CB and Choung J (2017) Fatigue damage analysis for a floating offshore wind turbine mooring line using the artificial neural network approach. *Ships and Offshore Structures* 12(sup1): S288–S295.
- Li CB, Choung J and Noh MH (2018) Wide-banded fatigue damage evaluation of catenary mooring lines using various artificial neural networks models. *Marine Structures* 60: 186–200.
- Li Z, Xia B, Zhang J, et al. (2022) A comprehensive survey on data-efficient GANs in image generation. *arXiv preprint arXiv:2204.08329*.
- Łuczak D (2024) Machine fault diagnosis through vibration analysis: time series conversion to grayscale and RGB images for recognition via convolutional neural networks. *Energies* 17(9): 1998.
- Ma KT, Shu H, Smedley P, et al. (2013) A historical review on integrity issues of permanent mooring systems. In: *Offshore Technology Conference*. OTC, OTC–24025.
- Maeda H, Kashiyama T, Sekimoto Y, et al. (2021) Generative adversarial network for road damage detection. *Computer-Aided Civil and Infrastructure Engineering* 36(1): 47–60.
- Mendoza N, Robertson A, Wright A, et al. (2022) Verification and validation of model-scale turbine performance and control strategies for the IEA Wind 15 MW reference wind turbine. *Energies* 15(20): 7649.

- Odena A (2016) Semi-supervised learning with generative adversarial networks. arXiv preprint arXiv:1606.01583.
- Radford A, Metz L and Chintala S (2015) Unsupervised representation learning with deep convolutional generative adversarial networks. arXiv preprint arXiv:1511.06434.
- Robertson A, Jonkman J, Masciola M, et al. (2014) Definition of the semisubmersible floating system for phase ii of oc4. Technical Report. National Renewable Energy Lab.(NREL).
- Saad AM, Schopp F, Barreira RA, et al. (2021) Using neural network approaches to detect mooring line failure. *IEEE Access* 9: 27678–27695.
- Sharma S and Nava V (2024) Condition monitoring of mooring systems for floating offshore wind turbines using convolutional neural network framework coupled with autoregressive coefficients. *Ocean Engineering* 302: 117650.
- Sidarta DE, O’Sullivan J and Lim HJ (2018) Damage detection of offshore platform mooring line using artificial neural network. In: *International Conference on Offshore Mechanics and Arctic Engineering*. American Society of Mechanical Engineers, Vol. 51203, V001T01A058.
- Tamuly P, Sharma S and Nava V (2025) Integrated damage detection and time-series data augmentation for floating offshore mooring systems via variational semi-supervised learning. *Ocean Engineering* 330: 121199. <https://www.sciencedirect.com/science/article/pii/S0029801825009126>
- Tang Z, Chen Z, Bao Y, et al. (2019) Convolutional neural network-based data anomaly detection method using multiple information for structural health monitoring. *Structural Control and Health Monitoring* 26(1): e2296.
- Tarawneh AS, Hassanat AB, Altarawneh GA, et al. (2022) Stop oversampling for class imbalance learning: a review. *IEEE Access* 10: 47643–47660.
- Van der Maaten L and Hinton G (2008) Visualizing data using t-sne. *Journal of Machine Learning Research* 9(11): 2579–2605.
- WindEurope (2023) Wind energy in Europe: 2022 statistics and the outlook for 2023-2027. Technical report, Windeurope.org.
- Yao J, Wu W and Li S (2022) Anomaly detection model of mooring system based on lstm pca method. *Ocean Engineering* 254: 111350.
- Yee X, Mohamed M and Montasir O (2021) Application of artificial neural network on health monitoring of offshore mooring system. In: *IOP Conference Series: Materials Science and Engineering*. IOP Publishing, Vol. 1144, 012035.